Available online at www.sciencedirect.com
ScienceDirect
Materials Chemistry and Physics 105 (2007) 320–324
MATERIALS CHEMISTRY AND PHYSICS
www.elsevier.com/locate/matchemphys

Exaggerated grain growth in Ni-doped $BaTiO_3$ ceramics

Y.C. Huang, W.H. Tuan *

Department of Materials Science and Engineering, National Taiwan University, Taipei 106, Taiwan

Received 12 July 2006; received in revised form 11 April 2007; accepted 29 April 2007

Abstract

With approximately 0.7 mol% Ni doping, the formation of hexagonal phase in $BaTiO_3$ after sintering at a temperature above 1385 °C in air has been observed. The shape of the h-$BaTiO_3$ grains is plate-like, and the length of these h-$BaTiO_3$ plates can be longer than 15 mm. As the amount of Ni doping increases above or decreases below 0.7 mol%, the hexagonal phase disappears and the resulting microstructure is dominated by small $BaTiO_3$ grains. This critical amount of Ni (i.e. 0.7 mol%) corresponds to the solubility of Ni in $BaTiO_3$. The exaggerated growth of the plate-like grains in $BaTiO_3$ relates strongly to the formation of oxygen vacancies due to the presence of Ni acceptors.

Keywords: $BaTiO_3$; NiO; Pressureless sintering; Grain growth; Solubility

1. Introduction

Barium titanate ($BaTiO_3$) is a ferroelectric material with high permittivity. The phase of $BaTiO_3$ at room temperature is a tetragonal phase, then transforms to cubic phase at 130 °C [1]. The phase transformation from cubic phase to tetragonal phase has received wide attention for its correlation with the ferroelectric characteristics of $BaTiO_3$. Apart from cubic and tetragonal phases, $BaTiO_3$ can also be present as other crystalline forms. For example, a hexagonal phase is stable at a temperature higher than 1460 °C [1]. However, the attention given to the phase is relatively little.

Several studies indicated that the h-phase could be formed by sintering $BaTiO_3$ in a reducing atmosphere [2]; or by doping acceptors, such as Mg, Al, Cr, Mn, Fe, Co, Zn, Ga, Ni, In, Cu, etc. [3–7]. The vacancy concentration within $BaTiO_3$ increases with the decrease of oxygen partial pressure in the sintering atmosphere [8]. The addition of acceptors also induces the formation of vacancies [9]. To increase the concentration of oxygen vacancy is the key to the formation of hexagonal phase. A recent study indicated that polycrystalline h-$BaTiO_3$ could be used as microwave component [10]. However, the microwave characteristics of h-$BaTiO_3$ single crystal are not yet available. It is therefore of interest to prepare the h-$BaTiO_3$ single crystal.

Tetragonal $BaTiO_3$ tends to form large grains with equiaxed features at elevated temperatures, especially when a small amount of Ti-rich phase is present [11]. Many researchers had taken the advantage of this behavior to produce large $BaTiO_3$ single crystal by using pressureless sintering. The dimensions of t-$BaTiO_3$ single crystal can reach 10 mm [12].

The shape of h-$BaTiO_3$ grains is plate-like [13]. However, the size of such h-phase grains depends strongly on the sintering atmosphere and the amount of acceptors. To the best knowledge of the present authors, the size of the h-$BaTiO_3$ grains can be produced by pressureless sintering in previous studies is less than 150 μm.

The objective of the present study is to produce large h-$BaTiO_3$ grains by using pressureless sintering in air. In order to achieve this target, a small amount of NiO is added into $BaTiO_3$. The processing conditions to produce such large h-phase grains are reported here. The electrical properties of the h-$BaTiO_3$ single crystal will be discussed in a separate report.

2. Experimental procedure

Barium titanate powder (NEB, Product No. 52909, Ferro Co., USA) and various amount of nickel nitrate (ACROS Organics Co., USA) were tumble milled together in ethyl alcohol for 4 h. The Ba/Ti ratio of the $BaTiO_3$ powder as reported by the manufacturer was 1.000 ± 0.002. The total amount of other impurities (SrO ~ 150 ppm, CaO ~ 20 ppm, Fe_2O_3 ~ 70 ppm, SiO_2 ~ 75 ppm, Al_2O_3 ~ 75 ppm) was less than 400 ppm. The grinding media used was zirconia balls. The slurry of the powder mixtures was dried using a rotary evaporator. The dried lumps were then crushed and passed through a plastic sieve. The powder was calcined in air at 500 °C for 2 h to remove the nitrate; then the

* Corresponding author. Tel.: +886 2 23659800; fax: +886 2 23634562.
E-mail address: tuan@ccms.ntu.edu.tw (W.H. Tuan).

0254-0584/$ – see front matter © 2007 Elsevier B.V. All rights reserved.
doi:10.1016/j.matchemphys.2007.04.075

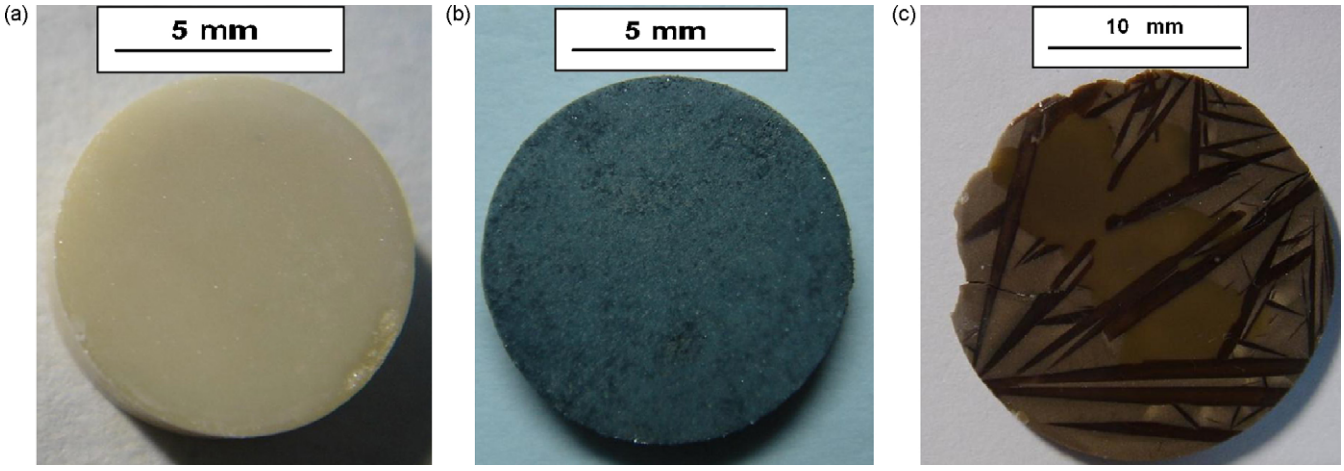

Fig. 1. Morphology of $BaTiO_3$ (a and b) and Ni-doped $BaTiO_3$ (c) specimens after sintering at 1400 °C in air for 2 h. The $BaTiO_3$ in (b) was sintered in a flowing H_2/N_2.

powder was sieved again. The powder was formed into disks by pressing uniaxially at 25 MPa. The size of the discs was 10 mm in diameter and about 3 mm in thickness. The sintering was performed in air at 1330–1400 °C for 2 h. The heating and cooling rates were 3 °C min^{-1}. For comparison purpose, several $BaTiO_3$ specimens were also prepared and sintered in a flowing gas mixtures of nitrogen (95%) and hydrogen (5%).

The density was determined by the water displacement method. The polished specimens were prepared by grinding with SiC particles and polishing with Al_2O_3 particles. The grain boundary was revealed by etching with a dilute solution of HCl and HF or by etching thermally at a temperature 100–120 °C below the sintering temperature for 30 min. The microstructure was observed by an optical microscope (OM) or a scanning electron microscope (SEM). The grain size was determined by applying an image analysis technique on the photos taken from OM or SEM. Phase identification was performed by X-ray diffractometry (XRD) at a scanning rate of 0.05° 2θ s^{-1}. A very slow scanning rate (0.002° 2θ s^{-1}) was also used to determine the lattice constants of *c* and *a* by using the (0 0 2) and (2 0 0) reflections. The *c*/*a* ratio was then obtained.

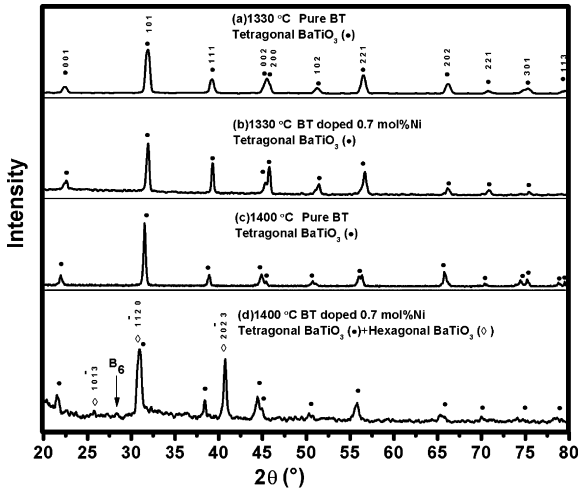

Fig. 2. XRD patterns of $BaTiO_3$ and Ni-doped $BaTiO_3$ specimens after sintering at 1330 °C or 1400 °C.

3. Results

XRD analysis reveals only tetragonal $BaTiO_3$ and NiO in the powder after the calcination at 500 °C. Fig. 1(a) and (b) show the surface of the $BaTiO_3$ samples after sintering at 1400 °C in air. The color of $BaTiO_3$ specimen, Fig. 1(a), is light brownish after sintering. However, the color of the $BaTiO_3$ specimen sintered in an oxygen-lean environment (flowing H_2/N_2) is dark blue (see Fig. 1(b)). The color of Ni-doped $BaTiO_3$ specimen is also very dark after sintering in air (Fig. 1(c)). Several large grains are long enough to spread across the entire cross-section of the disc. The maximum length of such large grains is around 15 mm, which is close to the diameter of the disc.

Fig. 2 shows the XRD patterns of $BaTiO_3$ and Ni-doped $BaTiO_3$ specimens after sintering at 1330 °C and 1400 °C in air. Only tetragonal phase is found in the $BaTiO_3$ specimens. After the addition of 0.7 mol% Ni, the tetragonal phase remains the only phase present in the specimen sintered at 1330 °C. However, a hexagonal phase is found as the major phase in the Ni-doped $BaTiO_3$ specimen as the sintering temperature is raised to 1400 °C. Furthermore, a small amount of $Ba_6Ti_{17}O_{40}$ (B6) phase is also found.

The values of *c*/*a* ratio are shown as a function of Ni content in Fig. 3. The ratio drops from 1.010 to a lower value of 1.004 as the Ni content is higher than 0.7 mol%, then stabilize at 1.004 with the further increase of Ni content. It indicates that Ni^{2+} ion

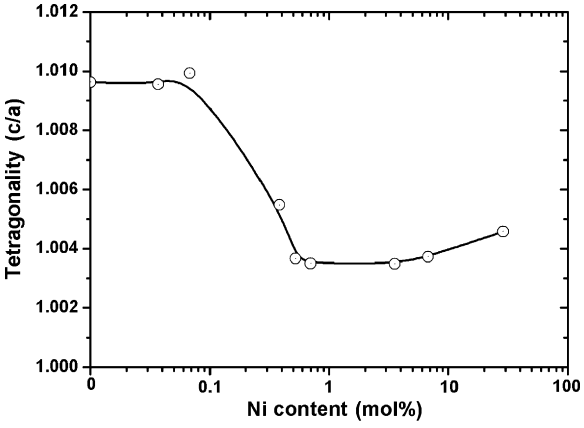

Fig. 3. Tetragonality (*c*/*a* ratio) of tetragonal $BaTiO_3$ as a function of Ni content.

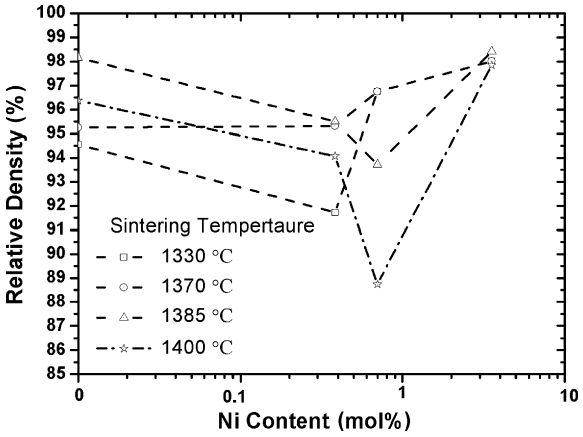

Fig. 4. Relative density of Ni-doped $BaTiO_3$ specimens as a function of Ni content.

is capable to dissolve into $BaTiO_3$ crystals and the solubility of Ni^{2+} ion in $BaTiO_3$ is 0.7 mol%.

The relative densities of the Ni-doped $BaTiO_3$ specimens are shown as a function of Ni content in Fig. 4. As the Ni content is lower than the solubility, the presence of Ni solute reduces the density of the specimens. The density reaches its lowest value as the Ni content is close to its solubility in $BaTiO_3$. As the Ni content is higher than the solubility, the density of all the specimens increases to a value of 98%, which shows little dependence on the Ni amount added.

Fig. 5 shows the microstructures of the $BaTiO_3$ specimens after sintering at 1330 °C and 1400 °C for 2 h in air. The $BaTiO_3$ specimen sintered at 1330 °C shows a typical bimodal microstructure for pure barium titanate specimens. The large grains in Fig. 5(a) are twinned $BaTiO_3$ grains and are larger than the untwined grains (the twin plane can be seen as a straight line crossing the large grains). At elevated temperature (above the eutectic temperature) the microstructure is dominated by twinned $BaTiO_3$ grains. There are no small grains present in the $BaTiO_3$ specimen sintered at 1400 °C. The coarse grains show equiaxed characteristics. Fig. 6 shows the microstructure of the 0.4 mol% Ni-doped $BaTiO_3$ specimens after sintering. In the specimen sintered at 1330 °C, the large grains are no longer existed as the small amount of Ni is added. As the sintering temperature increases to 1400 °C, the microstructure of the 0.4 mol% Ni-doped $BaTiO_3$ specimen is similar to that of the un-doped $BaTiO_3$ specimen sintered at 1400 °C, except that the size of the $BaTiO_3$ grains is slightly larger. As the Ni content increases to 0.7 mol%, the size of $BaTiO_3$ grains remains small as the sintering temperature is 1330 °C; however, several plate-like large grains are formed after sintering at 1400 °C (Fig. 7). The length of such plate-like grains reaches a value over 10 mm. As Ni content increases to 3.6 mol%, the size of $BaTiO_3$ grains remains small even when the sintering temperature is increased to 1400 °C (Fig. 8). Table 1 summarizes the dimensions of the $BaTiO_3$ grains in the $BaTiO_3$ and Ni-doped $BaTiO_3$ specimens. It demonstrates that the exaggerated grain growth is found only within a narrow composition range and above a certain sintering temperature. Since the sintering temperature is higher than the eutectic temperature of $BaTiO_3$ and TiO_2 [1]; a liquid phase is found in the Ni-doped $BaTiO_3$ specimens after sintering at about 1385 °C. The liquid phase mainly locates at the boundaries of $BaTiO_3$ grains.

4. Discussion

There are many techniques available to produce single crystals; however, the pressureless sintering is the most economically

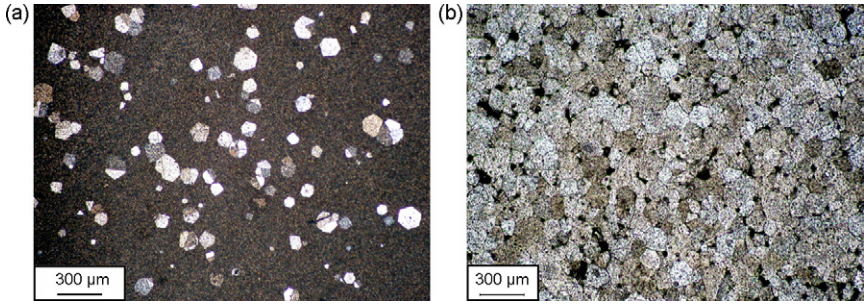

Fig. 5. Micrographs of $BaTiO_3$ specimens after sintering at 1330 °C (a) and 1400 °C (b).

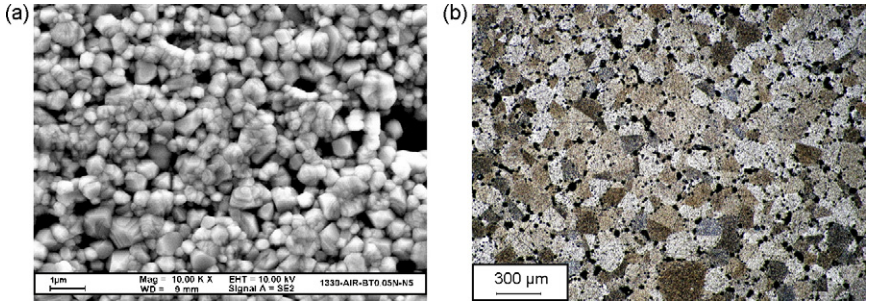

Fig. 6. Micrographs of 0.4 mol% Ni-doped $BaTiO_3$ specimens after sintering at 1330 °C (a) and 1400 °C (b).

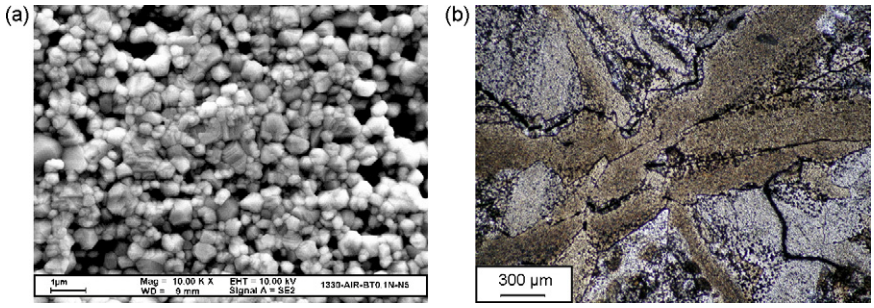

Fig. 7. Micrographs of 0.7 mol% Ni-doped $BaTiO_3$ specimens after sintering at 1330 °C (a) and 1400 °C (b).

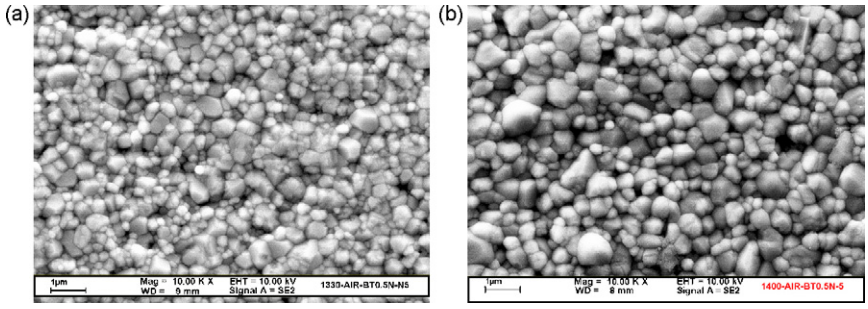

Fig. 8. Micrographs of 3.6 mol% Ni-doped $BaTiO_3$ specimens after sintering at 1330 °C (a) and 1400 °C (b).

viable process. Nevertheless, the size of the single crystal can be prepared by applying this technique is relatively small, less than 10 mm, as reported in the previous studies [4,5,13]. It is interesting to note that the size of the plate-like $BaTiO_3$ grains prepared in the present study seems to depend strongly on the size of the specimen. We could always observe some large grains grow from one end of the disc to another end. As the diameter of disc is 8 mm, the maximum length of the large grain is close to 8 mm; as the diameter of the disc is 15 mm, the largest grain can then reach 15 mm (see Fig. 1(c)).

Several techniques have been employed to determine the solubility of various dopants in $BaTiO_3$ [14–16]. The most popular analysis techniques involve the measurement of the Curie temperature and lattice parameter. However, the Curie temperature of dielectric is affected by many factors, such as the presence of internal stress, external stresses and microstructural characteristics [16]. To determine the solubility by measuring the lattice parameters has thus received wide popularity. In the present study, the *c*/*a* ratio is used instead of the lattice parameters of *c* and *a*. The two peaks, (0 0 2) and (2 0 0), used in the present study to determine the *c*/*a* ratio are very close to each other, therefore a calibration is no longer needed to ensure the accuracy for the *c*/*a* values.

In the present study, the hexagonal $BaTiO_3$ phase starts to form at a temperature as low as 1385 °C. This temperature is lower than the temperature used in the previous study to prepare h-$BaTiO_3$. In their study, a minimum temperature of 1400 °C was used [5]. Though the temperature used in the present study is relatively low, the addition of a certain amount of Ni, around 0.7 mol%, is essential for the formation of hexagonal phase. This critical amount is close to the solubility of Ni in $BaTiO_3$.

The solubility of a dopant in $BaTiO_3$ depends not only on the charge but also on the radius of the dopant [14]. Though the charge of Ni^{2+} ion is the same as that of Ba^{2+}, the radius of Ni^{2+} ion (0.069 nm) is close to that of Ti^{4+} ion (0.0605 nm) instead [17]. Therefore, Ni^{2+} ion is possible to substitute Ti^{4+} ion, such as the reaction shown below:

$$\mathrm{Ni} \xrightarrow{\mathrm{BaTiO_3}} \mathrm{Ni}''_{\mathrm{Ti}} + \mathrm{Vo}^{\bullet\bullet} \quad (1)$$

Table 1
Size of $BaTiO_3$ grains in $BaTiO_3$ and Ni-doped $BaTiO_3$ specimens after sintering at the indicated temperatures in air for 2 h

	1330 °C (μm)	1370 °C (μm)	1385 °C (μm)	1400 °C (μm)
0 mol% Ni	N: 0.98 ± 0.47(t), A: 106 ± 41(t)	250 ± 138(t)	180 ± 66(t)	160 ± 56(t)
0.4 mol% Ni	0.61 ± 0.16(t)	170 ± 76(t)	210 ± 74(t)	200 ± 55(t)
0.7 mol% Ni	0.42 ± 0.18(t)	0.35 ± 0.18(t)	L: 4780 ± 2500(h), W: 370 ± 160(h), N: 35 ± 19(t)	L: 3130 ± 2600(h), W: 650 ± 350(h), N: 33 ± 16(t)
3.6 mol% Ni	0.36 ± 0.18(t)	0.47 ± 0.22(t)	0.40 ± 0.18(t)	0.40 ± 0.19(t)

$BaTiO_3$ modification is indicated in parenthesis. The diameter of the specimen is 8 mm. *Note*: N: size of normal grains; A: size of abnormal grains; L: length of plate-like grain; W: width of plate-like grain; t: tetragonal phase; h: hexagonal phase.

Since the charge of Ni^{2+} ion is lower than that of Ti^{4+} ion, the Ni ion acts as the acceptor to $BaTiO_3$. Furthermore, the oxygen vacancy is needed to compensate the substitution of Ti^{4+} ion with Ni^{2+} ion. As the Ni content is close to the solid solution limit, the concentration of oxygen vacancy also reaches its highest value. The solubility of Ni in $BaTiO_3$ is as high as 0.7 mol%, from Eq. (1), the concentration of oxygen vacancy is the same as that of Ni solute. It thus suggests that an amount of 7000 ppm oxygen vacancy is formed due to the solution of Ni into $BaTiO_3$. Since there is no h-phase found in the un-doped $BaTiO_3$ specimens as they are sintered at 1400 °C in a flowing H_2/N_2, indicating that the reducing atmosphere is not low enough to generate an equivalent amount of oxygen vacancy. The addition of acceptor is thus an effective method to produce a relatively large amount of oxygen vacancy.

As the Ni content is lower than the solubility, the presence of the Ni^{2+} solutes slows down the densification of $BaTiO_3$; nevertheless, enhances its grain growth. The grain size of the Ni-doped $BaTiO_3$ specimens sintered at 1330 °C is small; it may be resulted from their low density. Raising the sintering temperature can compensate the decrease of densification. However, the density of the 0.7 mol% Ni-doped $BaTiO_3$ specimen after sintering at 1400 °C is still low (see Fig. 4). It is contributed by the formation of many cracks (see Fig. 7), which may correlate to the formation of hexagonal phase.

As the Ni content is higher than the solubility limit, the growth of large $BaTiO_3$ grains is prohibited. As stated above, the addition of fine NiO particles introduces many vacancies into $BaTiO_3$. However, the increase of NiO particles may also increase the number of nuclei of large grains. The number of these nuclei may be too high to allow their growth. The size of the $BaTiO_3$ grains is thus small after sintering. The transformation from tetragonal to hexagonal phase is also not observed. There is a strong connection between the presence of large grain and the formation of hexagonal phase. It seems that the formation of large grain triggers the phase transformation. The possible reason needs further investigation.

The formation of a liquid phase (B6) seems also helpful to the growth of large grains. The solution of Ni ion into $BaTiO_3$ pushes a little bit amount Ti ion out of the crystal into grain boundary area as the reaction shown below:

$$BaTiO_3 + xNiO \rightarrow Ba(Ti_{1-x}Ni_x)O_{3-x} + xTiO_2 \quad (2)$$

The higher Ti concentration facilitates the formation of the liquid phase at grain boundary. The liquid phase provides a fast mass transportation path; the grain growth is therefore fast as the liquid phase is formed.

5. Conclusions

In the present study, the $BaTiO_3$ specimens with large plate-like grains $\geq$15 mm are prepared by pressureless sintering in air. An addition of 0.7 mol% of Ni is essential to the formation of large grains. The critical content corresponds to the solid solution limit of Ni in $BaTiO_3$. The Ni ion acts as the acceptor and induces the increase of oxygen vacancy concentration. The vacancy concentration reaches its highest value as the Ni addition approaches its solubility. The large amount of oxygen vacancy helps the formation of h-$BaTiO_3$ and large plate-like grains.

References

[1] K.W. Kirby, B.A. Wechsler, J. Am. Ceram. Soc. 74 (1991) 1841.
[2] A. Rečnik, D. Kolar, J. Am. Ceram. Soc. 79 (1996) 1015.
[3] R.M. Glaister, H.F. Kay, Proc. Phys. Soc. 76 (1960) 763.
[4] H.T. Langhammer, T. Müller, K.H. Felgner, H.P. Abicht, J. Am. Ceram. Soc. 83 (2000) 605.
[5] M.H. Lin, H.Y. Lu, Philos. Mag. A 81 (2001) 181.
[6] H.T. Langhammer, T. Müller, R. Bottcher, H.P. Abicht, Solid State Sci. 5 (2003) 965.
[7] G.M. Keith, M.J. Rampling, K. Sarma, N.Mc. Alford, D.C. Sinclair, J. Eur. Ceram. Soc. 24 (2004) 1721.
[8] N.H. Chan, R.K. Sharma, D.M. Smyth, J. Am. Ceram. Soc. 64 (1981) 556.
[9] N.H. Chan, R.K. Sharma, D.M. Smyth, J. Am. Ceram. Soc. 65 (1982) 167.
[10] S.F. Wang, Y.C. Hsu, J.P. Chu, C.H. Wu, Appl. Phys. Lett. 88 (2006) 042909.
[11] Y.K. Cho, S.J.L. Kang, D.Y. Yoon, J. Am. Ceram. Soc. 83 (2004) 119.
[12] H.Y. Lee, J.S. Kim, D.Y. Kim, J. Eur. Ceram. Soc. 20 (2000) 1595.
[13] D. Kolar, U. Kunaver, A. Rečnik, Phys. Stat. Sol. A 166 (1998) 219.
[14] D. Makovec, Z. Samardzija, M. Drofenik, J. Am. Ceram. Soc. 87 (2004) 1324.
[15] S.J. Shih, W.H. Tuan, J. Am. Ceram. Soc. 87 (2004) 401.
[16] H.J. Hwang, T. Nagai, T. Ohji, M. Sando, M. Toriyama, K. Niihara, J. Am. Ceram. Soc. 81 (1998) 709.
[17] R.D. Shannon, Acta Crystallogr. A: Found. Crystallogr. 32 (1976) 751.